XXXVI Ibero-Latin American Congress on Computational Methods in Engineering
CILAMCE
Rio de Janeiro, 22-25 Nov 2015

STOCHASTIC HETEROGENEOUS APPROACH FOR WAVE PROPAGATION IN BALLASTED RAILWAY TRACK

Lúcio de Abreu Corrêa

Régis Cottereau

lucio.de-abreu-correa@centralesupelec.fr

regis.cottereau@centralesupelec.fr

Laboratoire MSSMat UMR 8579, CentraleSupelec, CNRS.

Grande Voie des Vignes, 92290, CHATENAY-MALABRY, France

Sofia Costa d'Aguiar

Charles Voivret

Estelle Bongini

Baldrik Faure

sofia.costadaguiar@sncf.fr

charles.voivret@sncf.fr

estelle.bongini@sncf.fr

baldrik.faure@sncf.fr

SNCF, Innovation & Research Dept.

40, Avenue des Terroirs de France, 75611 PARIS Cedex 12

Abstract. *Numerical models are commonly used to design and optimize the construction and operation of ballasted railways tracks. In this work, we used a randomly fluctuating continuum model to study the dynamical response of a ballast layer coupled to a homogeneous elastic half space. The simulations were performed using the Spectral Element Method. The comparison of the dispersion curves for a homogeneous and a heterogeneous ballast urges to consider apparently non-propagating modes in design. Those modes induce apparent damping in the free field.*

Keywords: *Stochastic modeling, Wave propagation, Granular media, Ballasted railway track*

1 INTRODUCTION

Strong competition with other means of transportation has increased the demand for performance in the railway industry. The dynamical loads caused by the passage of high-speed trains accelerate track deterioration and damage neighbor buildings (Connolly et al., 2014). Two classes of numerical models are used to try predict the behavior of these dynamical systems: (1) discrete approaches, in which each grain of the ballast is represented by a rigid body and interacts with its neighbors through nonlinear contact forces (using molecular dynamics or non-smooth contact dynamics); and (2) continuum approaches, in which the ballast is replaced by a homogenized continuum and the classical Finite Element Method (FEM, or similar) is used to solve the problem. The discrete approaches are today capable of solving only a few meters-length of ballast. The absence of an efficient scheme for parallelization over large clusters of computers remains an open problems.

However, in many cases, the microscopic behavior (found in discrete solution) is not the focus of attention *per se*, and some macroscopic feature are the only interesting, such as the settlement of a railway track. For these cases, it may prove appropriate to derive a so-called *macroscopic* model (Pasternak and Mühlhaus, 2005; Andrianov et al., 2010). The methods based on continuum mechanics (like the Finite Element Method) can solve very large models thanks to efficient parallelization schemes. However, a homogeneous continuum cannot represent the non-affine and heterogeneous fields of stress and strain present in the actual mechanical system.

The numerical simulation of dispersion curves in railway tracks is usually performed on homogeneous media (Sheng et al., 2004; Freitas da Cunha, 2013; Bian et al., 2015). The most advanced models consider 3D finite elements and model reduction (Arlaud et al., 2014). Unfortunately, these homogeneous models cannot reproduce accurately the experimental observations (Anbazhagan et al., 2011). It is necessary to consider the granular character of the material. The simulation of wave propagation in granular media for simple geometries has been treated using discrete models, and has succeeded in reproducing a wide range of experiments (Jia et al., 1999). The influence of pre-stress on the wave velocity in particular can be simulated (Shin and Santamarina, 2012) as well as the influence of the pressure in the grain network (Goddard, 1990). The simple addition of random ”heterogeneity” in a spring network allows to reproduce the complex frequency response seen in measurements of sound propagation in a granular system (Leibig, 1994). Note that Jia et al. (1999) observed the coexistence of an attenuated coherent signal and the ”coda”, which is a classical feature of seismic signals (Aki, 1969).

The objective of this work is use a statistical approach to model the mechanical properties of the ballast layer to build the dispersion curves of a ballasted railway track. This statistical approach aims to reproduce in a continuum model the heterogeneity of the stress field in a discrete granular model. The mechanical properties (in practice the Young's modulus) are modeled as stochastic random fields. This approach was introduced in (Cottereau et al., 2015) and we apply it here to the construction of dispersion curves of ballasted railway tracks in the frequency-wave-number domain. This representations allow a good visualization of the modes present in the ballast layer.

The transition from time-space to frequency-wave-number domain is performed using a two dimensional Fourier transform. An array of sensors is spatially distributed in a model and captures the displacement in all directions. This data is used to obtain the dispersion curves (frequency-wave-number domain). Different configurations are considered to represent a larger area of the frequency-wave-number space. The curves obtained for the heterogeneous are consistently compared to the classical ones, obtained with a homogeneous ballast.

2 Numerical model

2.1 Spectral Element Framework

The SEM is a generalization of the FEM based on the use of high-order piecewise polynomial functions. A crucial aspect of the method is its capability to provide an arbitrary increase in accuracy by simply increasing the algebraic degree of these functions (the spectral degree n).

Here we will just summarizing the key features of the SEM, (Komatitsch, 2005). We begin from the equilibrium differential equation of elastodynamics:

$$\rho\frac{\partial \mathbf{v}}{\partial t} = \nabla \cdot \sigma + \mathbf{F} \tag{1}$$

where $\mathbf{v}(\mathbf{x}, t)$ denotes the velocity at position $\mathbf{x}$ and time t, $\rho(x)$ is the density distribution, and $F(x,t)$ the external body force. The stress tensor σ is related to the strain tensor by the constitutive relation $\sigma = \mathbf{C} : \nabla\mathbf{u}$, where $\mathbf{C}$ denotes a fourth-order tensor and $\mathbf{u}$ is the displacement field. No particular assumptions are made regarding the structure of $\mathbf{C}$, which describes the elastic properties of the medium (even non-linear constitutive laws (Di Prisco et al., 2007)). As in the FEM, the dynamic equilibrium problem for the medium is written in a variational form in space. In time, this method uses an explicit second-order finite-difference scheme, which is conditionally stable and must satisfy the Courant condition.

The features of the SEM are as follows:

- The partition of the domain is similar to FEM. The model domain Ω is subdivided into a number of non-overlapping elements Ω_{el},$el = 1, ..., n_{el}$ such that $\Omega = \cup_{el=1}^{n_{el}}\Omega_{el}$ and $\cap_{el=1}^{n_{el}}\Omega_{el} = 0$
- The basis functions within the elements are Lagrange polynomials with degree n and interpolated in $n + 1$ nodes.
- The interpolation nodes are chosen to be the Gauss-Lobatto-Legendre (GLL) points, which are the nodes of the GLL quadrature.

Thanks to this numerical strategy, exponential accuracy of the method is ensured. An increase of the polynomial order leads to an exponential decreasing of the aliasing error. This property, called spectral precision, gives its name to the method.

The use of an orthogonal basis of Lagrangian functions associated with integration using the GLL quadrature leads to a diagonal mass matrix. This property enables to use an explicit time stepping in which the inverse mass matrix M^{-1} can be exactly and easily computed. This feature does not, naturally, occur in so-called hp-FEMs.

Inserting the polynomial interpolation and quadrature rules into the variational form of the equations of elastodynamics leads to a system of ordinary differential equations:

$$\mathbf{M}\dot{\mathbf{V}} = \mathbf{F_{ext}} - \mathbf{F_{int}}(\mathbf{U}) + \mathbf{F_{trac}}(\tau) \tag{2}$$

where $\dot{\mathbf{U}} = \mathbf{V}$, $\mathbf{U}$, $\mathbf{V}$ and τ are vectors containing the components of the displacement, velocity and traction at the global nodes, respectively. $\mathbf{M}$ is the mass matrix. The vectors $\mathbf{F_{ext}}$ and $\mathbf{F_{int}}$ contain the external and internal forces, respectively, and $\mathbf{F_{trac}}$ corresponds to the traction forces.

The main features of the software (SEM3D) used in this paper are:

- The capability of dealing with externally created 3D unstructured meshes;
- Handling the partitioning and load balancing of the computational domain using METIS (Karypis and Kumar, 1999) as an external library;
- Presence of absorbing boundary conditions (PML) in order to avoid boundary reflections;
- Computational scalability.

2.2 Mechanical properties

To build this stochastic continuum heterogeneous medium, used to model the ballast layer, we need to define two things: (1)first-order marginal law; and (2) a correlation model. The correlation model chosen here is based in the literature. The first-order marginal law for the Young Modulus was identified using a optimization process when one discrete model was compared with one stochastic continuous one. For this task a conventional FEM was employed.

2.2.1 Discrete Model

The model consists of 29 cylinders with a radius of 35 cm and a height of 39 cm. Samples were taken from this cylinders as 48X48X32 cm^3 orthogonal parallelepiped. The total number of particles in each cylinder is around 2700. The particles are convex polyhedra with diameters between 2.5 cm and 5 cm, whose shapes have been obtained by digitalization from real ballast. An isotropic confinement pressure of 60 kPa is applied on all samples, a vertical load on the upper face of 63 kN, and the gravity is considered within all samples. The model was calculated using non-smooth contact dynamics (NSCD).

2.2.2 Continuum Model

The continuum model has one cubic sample of 48X48X35 cm^3, taken from cylinders with radius of 35 cm and 39 cm high. A radial pressure of 60 kPa is applied, a pressure of 163 kPa was applied on the upper face. Gravity is considered, the density was assumed as 1500 kg/m^3. In terms of first-order marginal law, we will model Youngs modulus field with a log-normal distribution. This model requires the definition of a mean value $\bar{E}$, a variance σ^2, and a correlation model. We took $\bar{E} = 80$ MPa given by the report (INNOTRACK D2.1.3, 2009), made in the INNOTRACK Project, variance (estimate below) and correlation length. (Quintanilla, 1999) developed a theoretical correlation model that was used here to estimate the correlation function, based in the Percus-Yevick model, the characteristic diameter was took as 4 cm. The value of the Poisson ratio was taken from the report (INNOTRACK D2.1.3, 2009), as $\nu = 0.23$. The boundary conditions are equal to those of the discrete model.

2.2.3 Identification Process

This task requires some measurement comparisons between the discrete and the continuum media. We choose the stress as comparison variable. This choice try to represent the same statistical behavior between the discrete and continuum media.

The forces in a granular model are point forces localized at the interface between grains. It is interesting to define a generalization of the notion of stress tensor for these granular media. Several proposals have been made by (Drescher and de Josselin de Jong, 1972; Rothenburg and Bathurst, 1989; Moreau, 1997) for the static regime.

Given a network of contact forces f_α^c (at contact points c and with coordinates α) in a granular medium, the equivalent stress field were used by (Love, 1927; Voivret, 2008), and can be defined as:

$$\sigma_{\alpha\beta}^V = \frac{1}{Vol} \sum_{c=1}^{N_c} f_\alpha^c \ell_\beta^c = n_c \langle f_\alpha \ell_\beta \rangle , \tag{3}$$

where ℓ^c is the vector linking the centers of the two particles in contact at c, the sum is on the N_c contact points in the averaging volume V, and $n_c = N_c/V$ is the density of contacts, see (Weber, 1966) for more details. Obviously, this quantity depends on the size of the averaging volume (with more variability over the whole sample for smaller volumes).

Now, we compare the probability density function obtained from the discrete model (reference) and the continuous (target) using a classical L2 norm. To measure the distance one norm was used the classical L^2 norm: (Arnst and Ghanem, 2008):

$$L_r = \int_{\Re+} \left(p\left(x\right) - p_r\left(x\right)\right)^2 dx, \tag{4}$$

where $p_r\left(x\right)$ is the probability density function of the discrete model and $p\left(x\right)$ is the probability density function of the continuum model.

The stochastic field was generated by spectral representation following the work made by (Shinozuka and Deodatis, 1991). This corresponds to the "RF Lib" that generates the Young's Modulus seen in the Fig. 1. This figure is a small schema of the algorithm used to minimize the distance between the first-order marginal.

One realization of the random Young Modulus was inserted in a classical FEM model. The stress distribution found in this model is compared using the Eq. 4. The optimization process was made using a Nelder-Mead simplex algorithm (Lagarias et al., 1998).

The identification results are plotted in the Fig. 2. The minimum distance is at $\sigma_E^2/\bar{E}^2 \approx 5.4$. For this variance a comparison of the stress distribution in log-log scale was presented in the Fig. 2, where a good approximation for the values around the mean was noted, the exponential behavior was well fitted, however the match in the tails was not perfect.

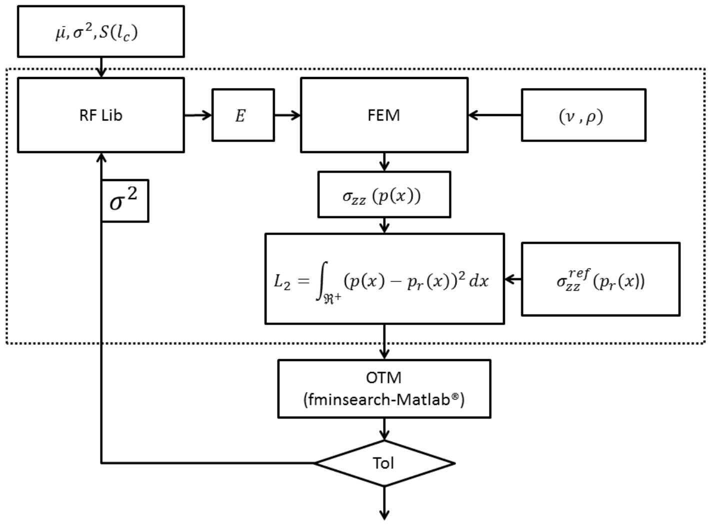

Figure 1: Material identification schema. The region inside the dot line represent the optimization loop.

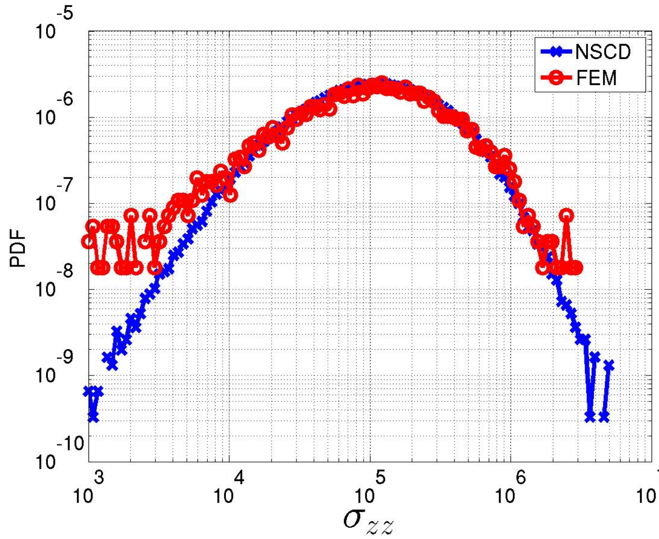

Figure 2: Relative distance between the probability distribution function σ_{zz} with $Vol = 8^3 cm^3$. Comparison of the probability distribution function with normalized variance $\sigma_E^2/\bar{E}^2 \approx 5.4$

2.3 Geometry and boundary conditions

Three models were built, one of those models can be seen in the Fig.3, it was based in a 250000 elements, with 375 degree of freedoms in each element, given $\approx$ 94x10^6 degrees of freedom. This model is 32 meters long. One prescribed force was impose as excitation. A rickers pulse with amplitude 1 and central frequency 30 Hz, for the other models the central frequency were modified. The Fig. 3 show also the region where vertical load is applied in the top of the ballast layer, and the mesh used. This kind of load condition was used in order to excite the "same modes" that the train usually applied in the ballast layer.

The other two models had 320000 and 380000 elements with 120x10^6 and 142x10^6 degrees of freedom. They only difference is the length of the railway, one is 40 and the other 48 meters long. The excitation for this models are 100 and 210Hz. Due the large number of degree of

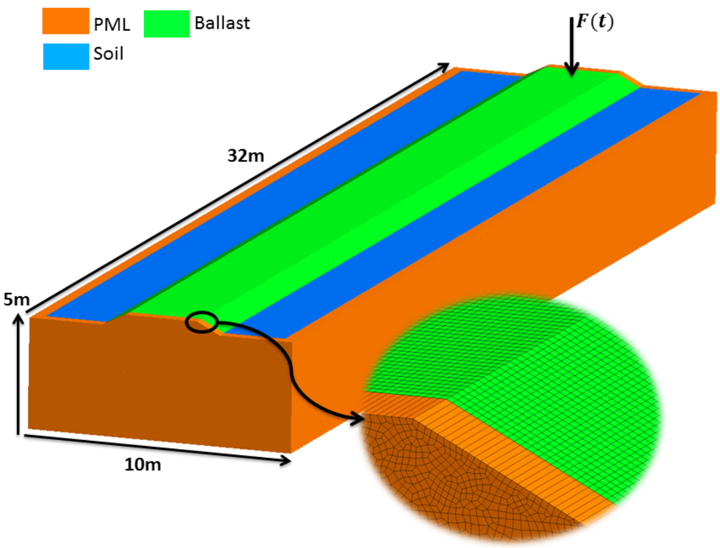

Figure 3: Geometry, mesh, and boundary conditions for the wave propagation analysis.

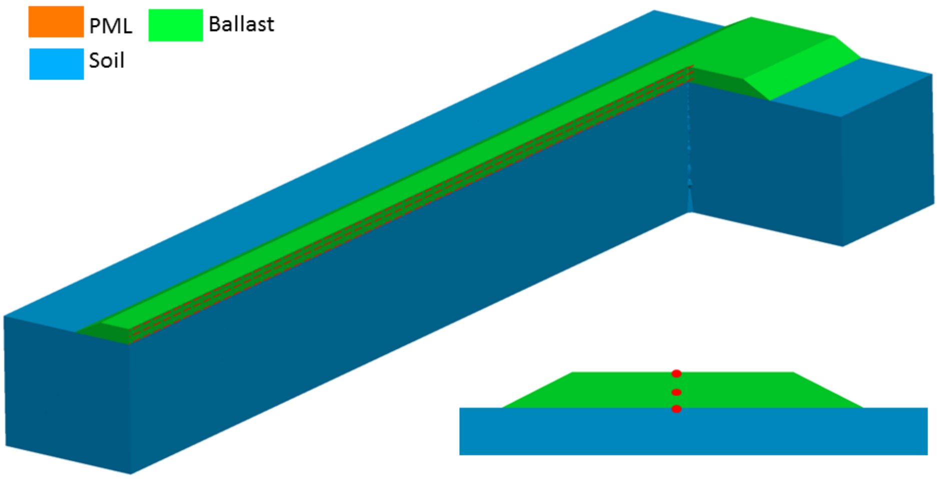

Figure 4: Cut view of the geometry and position of the captures lines. The red lines corresponds to the position of the captures lines. Three different sets where plotted at the top of the ballast, in the half of the layer, and on the interface between soil and ballast.

freedoms present in the model we choose a parallelizable and scalable code. This code, called SEM3D, it solve the dynamic equation in a time domain, using a explicit time integration, (Komatitsch et al., 2002), as described above.

Two kind of simulations were performed in each model, homogeneous and heterogeneous for the ballast material. The statistical mean of the mechanical properties was keep the same in this two models.

The Fig.4 show these position of the captures used to record the displacement field in the model. Three rows of captures were put inside of the ballast co-linear to the longitudinal axis, placed in the top, half, and the bottom of the ballast layer.

The mechanical properties used in the soil are the follow: $V_s = 180$m/s, $V_p = 1100$m/s, and $\rho = 1900$kg/m^3.

3 Influence of the heterogeneity on the dispersion curves

The study about the influence of heterogeneity in the dispersion curves can be derived from the equilibrium equation (1) where the stress is: $\sigma = \lambda(\mathbf{x})\mathrm{Tr}\epsilon\mathbb{I} + 2\mu\epsilon$, for one isotropic material, with the linear strain assumption: $\epsilon = (\nabla\mathbf{u} + \nabla\mathbf{u}^T)/2$. Assuming that the displacement field is expressed by $\mathbf{u} = \tilde{\mathbf{u}} \exp i(\mathbf{k}\cdot\mathbf{x} - \omega t)$, we obtain:

$$\left[(\lambda+\mu)\mathbf{k}\otimes\mathbf{k} - i(\nabla\lambda\otimes\mathbf{k} + \mathbf{k}\otimes\nabla\mu) + (\mu|\mathbf{k}|^2 - i\mathbf{k}\cdot\nabla\mu - \rho\omega^2)\mathbb{I}\right]\tilde{\mathbf{u}} = \mathbf{0}, \tag{5}$$

where $\mathbf{k}$ are the wave number, and ω is the time frequency. Dividing by ρ the above expression, one obtains:

$$(\Gamma(\mathbf{k}) - \omega^2\mathbb{I})\tilde{\mathbf{u}} = \mathbf{0}, \tag{6}$$

where the $\Gamma(\mathbf{k})$ is the well Christoffel tensor, the dispersion equations are obtained by writing $\det(\rho\Gamma(\mathbf{k}) - \rho\omega^2\mathbb{I}) = 0$.

Unfortunately this equation has no "easy" analytically solution for heterogeneous stochastic properties fields even in a full space. Furthermore, the stress-free condition in the upper surface leads this solution to some very complicated dispersion relation, usually solve this equation isn't an easy task. For this reason we choose directly numerical models. Unfortunately, models like semi-analitycal finite elements (Nelson et al., 1971) or global matrix (Knopoff, 1964) fail to solve 3D heterogeneties.

3.1 2D Fourier Transform

The standard time domain methods for measuring the velocities of elastic stress waves generally require minimal signal processing and are very friendly tool to use/apply. One single mode can be easily resolved separately in time domain. The group velocity may be determined by measuring the time that a wave package takes to propagate between two positions. Besides, if the time record is composed of a number of superimposed wave-modes, it may not be possible to measure correctly the amplitudes or velocity of the waves modes. It is logical think if there are many wave modes with very similar group velocities, and in this case, a considerable propagation distance is required before they can be distinguish in the time domain.

The two-dimensional Fourier transform technique is an alternative method of measuring the dispersion curves of Lamb waves quantitatively. It overcomes the problems of multiple modes and dispersion by transforming the received amplitude-time record to amplitude-wave-number records at discrete frequencies, where individual Lamb waves may be resolved and their amplitudes measured.

The processing of the spatial-time data collected in the model was made using a 2D Fourier Transform. This method was proven as an efficient tool to distinguish wave guided modes (Alleyne and Cawley, 1991). The Eq. (7) is the 2D-Fourier transformation and the inverse transformation pair defined by Eq. (8);

$$\mathbf{U}(\omega, \mathbf{k}) = \int_{-\infty}^{+\infty} \int_{-\infty}^{+\infty} \mathbf{u}(\mathbf{x}, t) e^{-i(\mathbf{k}\cdot\mathbf{x}+\omega t)} d\mathbf{x} dt \tag{7}$$

$$\mathbf{u}(\mathbf{x}, t) = \frac{1}{2\pi} \int_{-\infty}^{+\infty} \int_{-\infty}^{+\infty} \mathbf{U}(\omega, \mathbf{k}) e^{i(\mathbf{k}\cdot\mathbf{x}+\omega t)} d\mathbf{k} d\omega \tag{8}$$

where $\mathbf{U}(\omega, \mathbf{k})$ the frequency spectrum and $\mathbf{u}(\mathbf{x}, t)$ the data collected in the numerical model.

On the other hand, the displacement data can be roughly described as:

$$\mathbf{u}(\mathbf{x}, t) = \sum_{m=1}^{n} \mathbf{u}^m(\mathbf{x}) = \sum_{m=1}^{n} \mathbf{F}^m \cdot \mathbf{E}^m e^{i(\mathbf{k^m}\cdot\mathbf{x}+\omega t)} \tag{9}$$

where $\mathbf{u}^m$ is the m-th wave guided mode. It can be decomposed in sum of the forces ($\mathbf{F}^m$), excitability ($\mathbf{E}^m$), and plane waves $e^{i(\mathbf{k^m}\cdot\mathbf{x}+\omega t)}$.

The force depends on the excitation pulse imposed by the boundary conditions. The excitability is a function of the power flow of the mode, in other words, depends of the velocity and stress field of the mode. The excitability play a hole as a kind of transfer function, it links the imposed boundary condition and the wave mode amplitude.

The methodology that we applied here allow us found the inner product between force and excitability. So, we are aware that only some modes will be found, because the load are applied in one preferential direction. Only modes with some similar stress profile will appear the our dispersion curves.

3.2 Numerical Results

The Fig. 5 shows the normalized displacement field for different time instants for the excitation equal to 30Hz. Where the first line show results for the homogeneous case, the second line show the heterogeneous case, this representation is the same for all the figures below. In the homogeneous case its clear the presence of just one mode, it can be see clearly in the figures. The heterogeneous model shows in this same case a small dispersion of the wave front. This dispersion appears even in when the correlation length of the medium is very small compare to wavelength ($\ell_c/\lambda = 0.016$)

The Fig. 6 show the normalized displacement field for different time instants for the excitation equal to 100Hz. The homogeneous case present the wave-guide behavior, and it can be noted the presence of the first wave front, similar to Fig. 5, followed by other modes. In the heterogeneous media the scattering take place: a huge scatter of the wave front can be identified, consistent with a reduction in the energy velocity of the wave.

The Fig. 7 shows the normalized displacement field for different time instants for the excitation equal to 210Hz. The homogeneous case present the wave-guide behavior, but differently from the 30Hz case, Fig. 5, a wave front is no longer present. In the heterogeneous media a

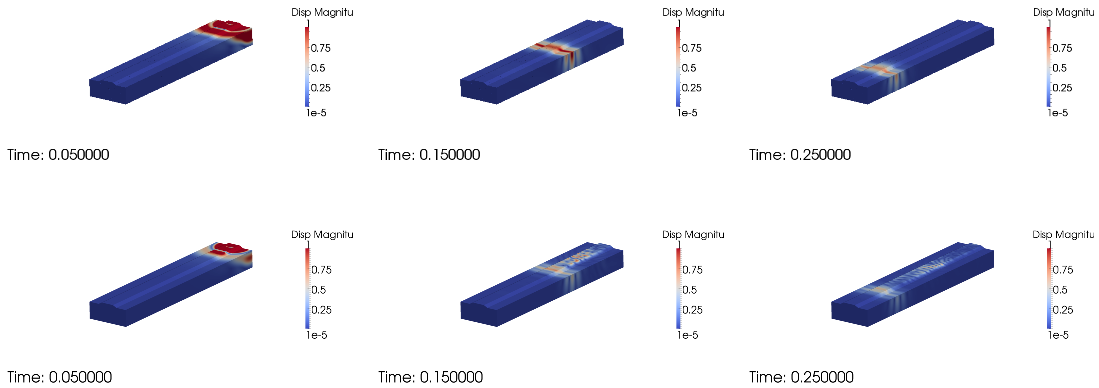

Figure 5: Normalized displacement field for the central frequency of 30Hz. The first line correspond to a homogeneous case, and the second one is for the heterogeneous case. Each column represent different time instants.

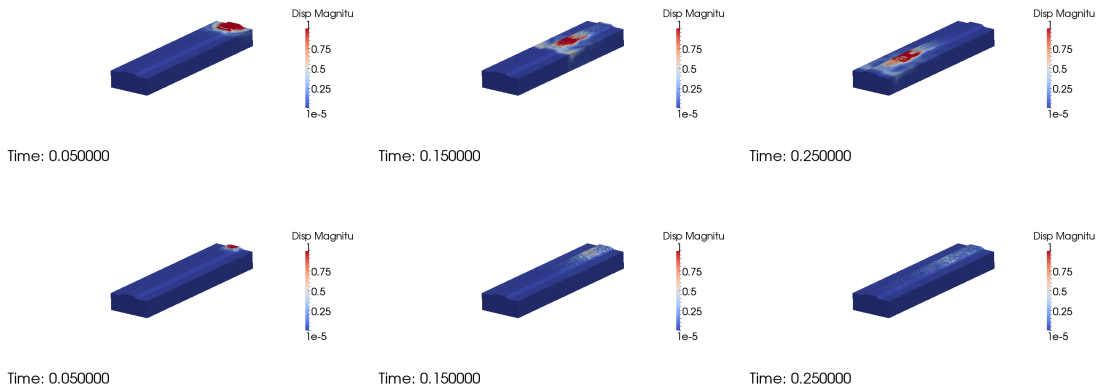

Figure 6: Normalized displacement field for the central frequency of 100Hz. The first line correspond to a homogeneous case, and the second one is for the heterogeneous case. Each column represent different time instants.

strong scattering wave regime occurs. The energy is completely scattered by the heterogeneities present in the medium. The energy velocity of the wave propagation are slower then the other models. This reduction is directly related to the ratio between correlation length and wavelength ($\ell_c/\lambda = 0.15$).

Finally, Fig. 8 shows the dispersion curve in a range frequency between 8 and 400Hz. They were created using the 3 models above. The sum of the displacement components were introduced in the Eq.(7). This field was plotted as a surface plot for the amplitudes higher than -60db. One deconvolution operation was performed to remove the influence of the source in all the models. In this figures, the black dotted line represent the shear wave velocity.

In the figure, is observable an amplitude gap between 60Hz and 150Hz for the homogeneous case,which is probably related to the low excitability for the modes in this region. Also for the homogeneous case, the convergence of the, approximately, 8 modes for the shear wave velocity appears very quickly. This is expected, since the excitation used produce predominantly shear stress, the energy conversion is more efficient to modes where shear stress is predominant.

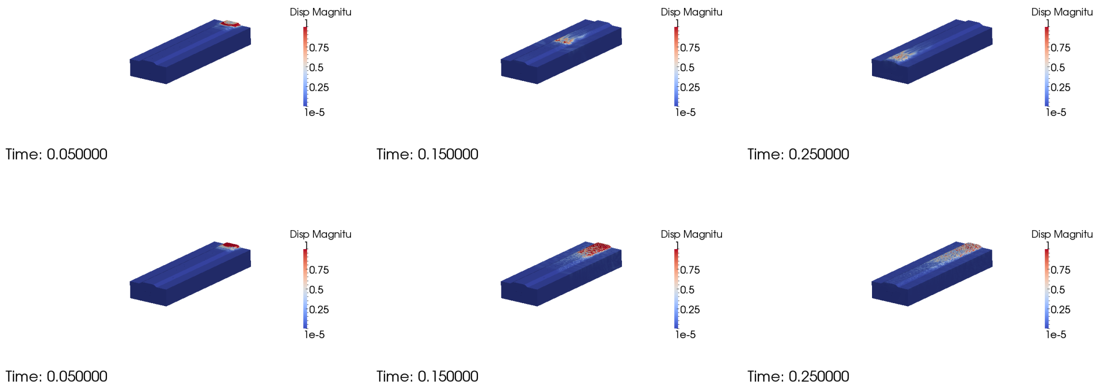

Figure 7: Normalized displacement field for the central frequency of 210Hz. The first line correspond to a homogeneous case, and the second one is for the heterogeneous case. Each column represent different time instants.

Other interesting behavior is the presence of some "spurious" mode in the low frequency with high velocity. In fact, this "spurious" mode is a longitudinal mode. More studies must be performed to understand this behavior. The difference between the modes that propagate in the top of the ballast are very similar to the modes in the interior. The difference is larger when we made one comparison between top and bottom. In the bottom of the ballast some interface wave appear, having a slightly greater speed than the shear velocity. The velocity in this case converge for Rayleigh velocity in the soil.

In the heterogeneous case was noted some kind of of energy leakage for the shear mode: the scattering and depolarization were the responsible for this effect. The reduction of velocity is easily noted in the frequencies greater then 100Hz, and with some difficult, two modes in this region can be distinguish. Other interesting feature of this model is the high attenuation of the frequencies higher than 250Hz. No displacement is present in this region. Unfortunately the concept of mode becomes very complex in heterogeneous media, as noted in the top and interior of the ballast. Finally in the interface between ballast and soil, some energy remains not so attenuated with velocity near to V_s.

4 Conclusions

One preliminary study was performed, the dispersion curves for homogeneous and heterogeneous media for one ballasted railway track were made. The dispersion curves in the homogeneous case present the classical behavior for wave guides, in the other hand the energy are distributed in a very large area in the heterogeneous case, making the classical analysis of modes more difficult. The behavior are related to the link between the correlation length of the medium and the wavelength, and it became more important when some threshold is achieved.

More studies must be performed to see if this threshold is related to the properties fluctuation in the medium. Other realizations of the stochastic random field used will be made in order to check this results, and the comparison with some semi-analytic model are necessary to validate the homogeneous approach.

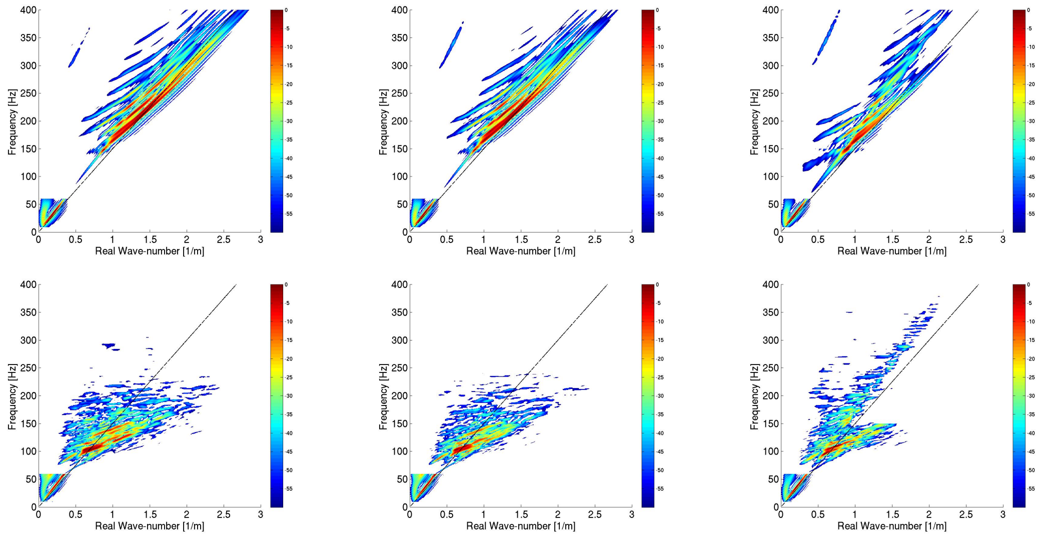

Figure 8: Dispersion curves for the ballast. In the upper line, dispersion curves for the top, half, and lower line respectively. The secound line present the same results for the heterogeneous case. The black dotted line represent the shear mode in a full space.

ACKNOWLEDGEMENTS

The spectral element software used for the simulation in this paper is developed jointly by CentraleSupélec, CEA Commissariat l'Energie Atomique and Institut de Physique du Globe de Paris. Within the SINAPS@ project, this development benefits from French state funding managed by the National Research Agency under program RNSR Future Investments bearing reference No. ANR-11-RSNR-0022-04.

References

K. Aki. Analysis of the seismic coda of local earthquakes as scattered waves. 74(2):615–631, 1969. doi: 10.1029/JB074i002p00615.

D. Alleyne and P. Cawley. A two-dimensional fourier transform method for the measurement of propagating multimode signals. *Journal of Acoustical Society of America*, 89(3):1159–1168, Março 1991.

P Anbazhagan, Buddhima N Indraratna, and G Amarajeevi. Characterization of clean and fouled rail track ballast subsurface using seismic surface survey method: Model and field studies. *Faculty of Engineering-Papers (Archive)*, pages 1–11, 2011.

I. V. Andrianov, J. Awrejcewicz, and D. Weichert. Improved continuous models for discrete media. 2010:986242, 2010. doi: 10.1155/2010/986242.

E Arlaud, S D'Aguiar, and E Balmes. Validation of a reduced model of railway track allowing long 3D dynamic calculation of train-track interaction. *Computer Methods and Recent Advances in Geomechanics*, (August):1193–1198, 2014. doi: 10.1201/b17435-209. URL `http://www.crcnetbase.com/doi/abs/10.1201/b17435-209`.

M. Arnst and R. G. Ghanem. Probabilistic equivalence and stochastic model reduction in multiscale analysis. 197:3584–3592, 2008. doi: 10.1016/j.cma.2008.03.016.

Xuecheng Bian, Chong Cheng, Jianqun Jiang, Renpeng Chen, and Yunmin Chen. Numerical analysis of soil vibrations due to trains moving at critical speed. *Acta Geotechnica*, pages 1–14, 2015.

D. P. Connolly, G. Kouroussis, O. Laghrouche, C. L. Ho, and M. C. Forde. Benchmarking railway vibrations - Track, vehicle, ground and building effects. *Construction and Building Materials*, August 2014. ISSN 09500618. doi: 10.1016/j.conbuildmat.2014.07.042. URL `http://linkinghub.elsevier.com/retrieve/pii/S0950061814007661`.

R. Cottereau, L. de Abreu Corrêa, J. C. Quezada, S. Costa d'Aguiar, and C. Voivret. Stochastic heterogeneous continuum modeling of a granular medium. Unpublished, 2015.

C Di Prisco, M Stupazzini, and C Zambelli. Nonlinear sem numerical analyses of dry dense sand specimens under rapid and dynamic loading. *International Journal for Numerical and Analytical Methods in Geomechanics*, 31(6):757–788, 2007.

A. Drescher and G de Josselin de Jong. Photoelastic verification of a mechanical model for the flow of a granular material. 20(5):337–340, 1972. doi: 10.1016/0022-5096(72)90029-4.

José Pedro Freitas da Cunha. *Modelling of Ballasted Railway Tracks for High-Speed Trains*. PhD thesis, Universidad do Minho, 2013.

J. D. Goddard. Nonlinear Elasticity and Pressure-Dependent Wave Speeds in Granular Media. *Proceedings of the Royal Society A: Mathematical, Physical and Engineering Sciences*, 430 (1878):105–131, 1990. ISSN 1364-5021. doi: 10.1098/rspa.1990.0083.

INNOTRACK D2.1.3. First phase on the modelling of poor quality sites. Technical Report Project no. tip5 ct-2006-031415, European commission - sixth framework program, 2009.

X. Jia, C. Caroli, and B. Velicky. Ultrasound Propagation in Externally Stressed Granular Media. *Physical Review Letters*, 82:1863–1866, 1999. ISSN 0031-9007. doi: 10.1103/PhysRevLett.82.1863.

George Karypis and Vipin Kumar. A fast and highly quality multilevel scheme for partitioning irregular graphs. *SIAM Journal on Scientific Computing*, 1999.

L. Knopoff. A matrix method for elastic wave problems. *Bulletin of the Seismological Society of America*, 54(1):431–438, 1964.

D. Komatitsch, J. Ritsema, and J. Tromp. The spectral-element method, Beowulf computing, and global seismology. *Science (New York, N.Y.)*, 298(5599):1737–42, November 2002. ISSN 1095-9203. doi: 10.1126/science.1076024. URL `http://www.ncbi.nlm.nih.gov/pubmed/12459579`.

Dimitri Komatitsch. The spectral-element method in seismology. *Geophysical Monograph Series*, 157(55):205–227, 2005. ISSN 0065-8448. doi: 10.1029/157GM13. URL `http://www.agu.org/books/gm/v157/157GM13/157GM13.shtml`.

J. C. Lagarias, J. A. Reeds, M. H. Wright, and P. E Wright. Convergence properties of the nelder–mead simplex method in low dimensions. *SIAM Journal on optimization*, 9(1):112–147, 1998.

Michael Leibig. Model for the propagation of sound in granular materials. *Physical Review E*, 49(2):1647–1656, 1994. ISSN 1063651X. doi: 10.1103/PhysRevE.49.1647.

A. E. H. Love. *A Treatise on the Mathematical Theory of Elasticity*. Number v. 4 in A Treatise on the Mathematical Theory of Elasticity. Cambridge University Press, 1927. ISBN 9781107618091. URL `https://books.google.fr/books?id=JFTbrz0Fs5UC`.

J.-J. Moreau. Numerical investigation of shear zones in granular materials. In P. Grassberger and D. Wolf, editors, *Proceedings of HLRZ-workshop on friction, arching, contact dynamics*. World Scientific, 1997.

R. B. Nelson, S. B. Dong, and R. D. Kalra. Vibrations and waves in laminated orthotropic circular cylinders. *Journal of Sound and Vibration*, 18(3):429–444, 1971.

E. Pasternak and H. B. Mühlhaus. Generalised homogenisation procedures for granular materials. *Mathematics and Mechanics of Granular Materials*, 52(1):199–229, July 2005. ISSN 00220833. doi: 10.1007/1-4020-4183-7_12. URL `http://link.springer.com/10.1007/s10665-004-3950-z`.

J. Quintanilla. Microstucture functions for random media with impenetrable particles. 60: 5788–5794, 1999. doi: 10.1103/PhysRevE.60.5788.

L. Rothenburg and R. J. Bathurst. Analytical study of induced anisotropy in idealized granular materials. 39:601–614, 1989.

X. Sheng, C.J.C. Jones, and D.J. Thompson. A theoretical study on the influence of the track on train-induced ground vibration. 272:909–936, 2004. ISSN 0022460X. doi: 10.1016/S0022-460X(03)00781-8. URL `http://dx.doi.org/10.1016/S0022-460X(03)00781-8`.

H. Shin and J. C. Santamarina. The Role of Particle Angularity on the Mechanical Behavior of Granular Mixtures. *Journal of Geotechnical and Geoenvironmental Engineering*, 139(2): 483, 2012. ISSN 1090-0241. doi: 10.1061/(ASCE)GT.1943-5606.0000768.

M. Shinozuka and G. Deodatis. Simulation of stochastic processes by spectral representation. 44(4):191–205, 1991. doi: 10.1115/1.3119501.

C. Voivret. *Texture et comportement des matériaux granulaires à grande polydispersité*. PhD thesis, Université Montpellier 2, 2008.

J. Weber. Recherches concernant les contraintes intergranulaires dans les milieux pulvérulents. *Bulletin de liaison des Ponts et Chaussées*, (20):1–20, 1966.